nopathy), whereas the remaining 47% showed unexpected post-receptoral dysfunction, such as cone (or cone-rod) dystrophy or RP. Thus, although the mechanism by which negative ERGs are induced remains unclear in VAD and hereditary photoreceptor disorders, post-receptoral dysfunction is strongly suspected to be a secondary effect.

With regard to cone dysfunction, considerable attention has been focused on which of the 3 cone classes is most susceptible to VAD. One report addresses this issue (4), finding that 2 of 3 patients with VAD had undetectable S-cone ERG responses, even though both these patients had borderline amplitude values in cone ERGs (4) with presumably preserved L- and M-cone function, findings which were similar to those in our present patient (Fig. 1B). To test the hypothesis that S-cone–mediated function is more severely affected than L- and M-cone–mediated function in VAD, we compared the results of SITA-SAP (Fig. 2A) with those of SITA-SWAP (Fig. 2C) in our patient. We noted that the MD values were much worse in SITA-SWAP than in SITA-SAP, suggesting that S-cone pathways were selectively affected before vitamin A treatment. Loss of the visual fields in SITA-SWAP was dramatically improved by vitamin A treatment (Fig. 2D). To our knowledge, this is the first report in which comparisons between white-on-white (SITA-SAP) and blue-on-yellow (SITA-SWAP) perimetries were performed before and after vitamin A treatment. Evaluation of both SITA-SAP and SITA-SWAP might be useful in clinical and diagnostic practice in patients with VAD. Taken together, our results support the hypothesis that S cones are indeed more vulnerable to VAD than L or M cones.

In conclusion, visual impairment due to VAD can be resolved with the application of appropriate therapy. Our findings suggest that rods and S cones are more susceptible to VAD than L or M cones. VAD should be considered as a potential cause of night blindness or unexplained visual loss, particularly in patients with clinically predisposing conditions, such as bile duct obstruction, malabsorption, or hepatic dysfunction.

Supported by grants from The Jikei University Research Fund (T.H.) and the Vehicle Racing Commemorative Foundation (T.H. and H.T.).

The authors report no proprietary interest.

Address for correspondence:
Takaaki Hayashi, MD, PhD
Department of Ophthalmology
The Jikei University School of Medicine
3-25-8 Nishi-shimbashi
Minato-ku, Tokyo, 105-8461, Japan
taka@jikei.ac.jp

REFERENCES

1. Saari JC. Biochemistry of visual pigment regeneration: the Friedenwald lecture. Invest Ophthalmol Vis Sci 2000; 41: 337-48.
2. Newman NJ, Capone A, Leeper HF, et al. Clinical and subclinical ophthalmic findings with retinol deficiency. Ophthalmology 1994; 101: 1077-83.
3. Hayashi T, Gekka T, Takeuchi T, Goto-Omoto S, Kitahara K. A novel homozygous *GRK1* mutation (P391H) in 2 siblings with Oguchi disease with markedly reduced cone responses. Ophthalmology 2007; 114: 134-41.
4. McBain VA, Egan CA, Pieris SJ, et al. Functional observations in vitamin A deficiency: diagnosis and time course of recovery. Eye 2007; 21: 367-76.
5. Koh AH, Hogg CR, Holder GE. The incidence of negative ERG in clinical practice. Doc Ophthalmol 2001; 102: 19-30.
6. Cideciyan AV, Jacobson SG. Negative electroretinograms in retinitis pigmentosa. Invest Ophthalmol Vis Sci 1993; 34: 3253-63.
7. Renner AB, Kellner U, Cropp E, Foerster MH. Dysfunction of transmission in the inner retina: incidence and clinical causes of negative electroretinogram. Graefes Arch Clin Exp Ophthalmol 2006; 244: 1467-73.

CLINICAL AND EXPERIMENTAL
OPTOMETRY

RESEARCH PAPER

Subfoveal choroidal thickness in multiple evanescent white dot syndrome

Clin Exp Optom 2012; 95: 212–217 DOI:10.1111/j.1444-0938.2011.00668.x

Ranko Aoyagi* MD
Takaaki Hayashi* MD PhD
Akiko Masai† MD
Katsuya Mitooka† MD PhD
Tamaki Gekka§ MD PhD
Kenichi Kozaki* MD PhD
Hiroshi Tsuneoka* MD PhD
* Department of Ophthalmology, The Jikei University School of Medicine, Tokyo, Japan
† Department of Ophthalmology, Daisan Hospital, The Jikei University School of Medicine, Tokyo, Japan
§ Department of Ophthalmology, Kashiwa Hospital, The Jikei University School of Medicine, Chiba, Japan
E-mail: taka@jikei.ac.jp

Submitted: 23 April 2011
Revised: 17 June 2011
Accepted for publication: 28 July 2011

Background: Multiple evanescent white dot syndrome (MEWDS) is an inflammation of the choriocapillaris, which typically presents with unilateral vision loss and is characterised by the presence of multiple yellow-white spots in the posterior pole to the midperipheral fundus. This study was conduced to evaluate subfoveal choroidal thickness between the acute and convalescent phases in two patients with MEWDS.
Methods: Two young female Japanese patients underwent a comprehensive ophthalmic examination, including slitlamp biomicroscopy, funduscopy and both fluorescein and indocyanine green angiographies. The subfoveal choroidal and central retinal thicknesses were measured using Cirrus high-definition spectral-domain optical coherence tomography.
Results: The two patients were diagnosed with unilateral MEWDS based on characteristic funduscopic and angiographic findings. The disrupted foveal inner segment–outer segment boundary line in the acute phase was restored in the convalescent phase in both patients. In the affected eye of Patient 1, the subfoveal choroidal thickness (337 μm) noted in the acute phase decreased to 249 μm at 133 days after the initial visit (convalescent phase). Similarly, the acute phase thickness (440 μm) in Patient 2 decreased to 358 μm at 133 days after the initial visit. The thickness in the asymptomatic opposite eye also decreased during the convalescent phase in both patients. In the acute phase, thickness in the affected eyes was greater than that in the opposite eyes in both patients. In contrast, central retinal thickness remained unchanged in both eyes during follow up in both patients.
Conclusion: This is the first report to describe the relationship between subfoveal choroidal thickness and MEWDS. We found that the choroid was thicker in the acute phase than the convalescent phase in both the affected and opposite eyes of both patients, suggesting that an inflammatory reaction might occur in the choroidal stroma in addition to the choriocapillaris and might be bilateral rather than unilateral.

Key words: choroidal inflammatory disease, choroidal thickness, optical coherence tomography, statins, white dot syndrome

Multiple evanescent white dot syndrome (MEWDS), first described in 1984 by Jampol and colleagues[1] and Sieving and colleagues,[2] is a typically unilateral retinopathy with sudden onset of vision loss that occurs predominantly in young females. Ophthalmoscopic examination in patients with MEWDS reveals multiple faint, yellow-white spots in the posterior pole to the midperipheral fundus. The disease is self-limiting with almost all patients regaining good visual acuity

within several weeks. Fluorescein angiography (FA) shows hyperfluorescence of the yellow-white spots, whereas late-phase indocyanine green angiography (ICGA) reveals more hypofluorescent spots than what is seen with fluorescein angiography.[3,4] Although the pathogenesis of MEWDS remains unknown, electroretinography and electrooculography have revealed dysfunction of the photoreceptors and retinal pigment epithelium.[5–7]

Recent spectral-domain optical coherence tomographic (SD-OCT) studies have noted disruptions in the photoreceptor inner segment/outer segment junction (IS/OS) in patients with acute phase MEWDS, but no pathological changes in the retinal pigment epithelium or choroid.[8,9] Here, we investigate changes in subfoveal choroidal thickness between acute and convalescent phases in two patients with MEWDS.

METHODS

This study was conducted under a retrospective design in two patients diagnosed with MEWDS. They had undergone a comprehensive ophthalmic examination, including assessment of visual acuity (VA), slitlamp biomicroscopy, dilated funduscopy and fluorescein angiography (VISUCAM NM/FA; Carl Zeiss Meditec AG, Dublin, CA, USA). We also performed indocyanine green angiography using a scanning laser ophthalmoscope Model 101 (Rodenstock Instruments, Munich, Germany) in one of the two patients.

Cross-sectional retinal images were evaluated using SD-OCT (Cirrus HD-OCT, Carl Zeiss Meditec AG) in both patients. The SD-OCT was taken horizontally through the centre of the fovea (6.0 mm line) using programs with either five-line raster or HD five-line raster. Using the Cirrus linear measurement tool, two independent observers manually measured subfoveal choroidal thickness from the posterior edge of the retinal pigment epithelium to the choroid/sclera junction at the position of the foveal depression, in accordance with a previously published method.[10] The average of the obtained measurements was determined as the subfoveal choroidal thickness. Similarly, the central retinal thickness (at the position of the foveal depression) was manually measured at this time to compare changes in both retinal and choroidal thickness during follow-up periods.

RESULTS

Patient 1

A 21-year-old female Japanese patient with no previous history of ocular disease presented to our hospital with sudden loss of visual acuity in the right eye. On initial examination, VA was 0.2 (with -11.00 DS) in the right eye and 1.2 (with -9.00 DS) in the left eye. No inflammatory cells were observed in the anterior segment or vitreous of either eye. Fundus examination revealed foveal granularity and scattered yellow-white spots in the posterior pole in the right eye (Figure 1A). Early phase fluorescein angiography in the right eye showed small hyperfluorescent lesions that were determined to be retinal spots (Figure 1B). Late-phase ICGA of the right eye revealed numerous hypofluorescent spots throughout the posterior pole (Figure 1C). In contrast, no significant findings were noted in the left eye on funduscopy, fluorescein angiography or indocyanine green angiography. SD-OCT of the right eye revealed a disrupted external limiting membrane (ELM) and IS/OS lines in the foveal region (Figure 2A). There was no evidence of systemic inflammation (normal erythrocyte sedimentation rate and C-reactive protein levels). No therapy was administered.

Five weeks after the initial visit, VA had recovered to 1.0, all evidence of foveal granularity and yellow-white spots had disappeared (Figure 1D) and the ELM and IS/OS lines had been restored without therapy. At the final visit (345 days after the initial visit), VA was 1.2 and ELM and IS/OS lines in the right eye were preserved (Figure 2C).

Patient 2

A 16-year-old female Japanese patient with a history of familial hypercholesterolaemia and simvastatin treatment was referred to our hospital three days after complaining of blurred vision in the right eye. She reported flu-like symptoms seven days before the initial visit. On initial examination, VA was 1.2 (-3.00 DS) in the right eye and 0.8 (-3.00 DS) in the left eye. No significant findings were observed in the anterior segment or vitreous of either eye. Funduscopy revealed foveal granularity and faint, scattered, yellow-white spots in the posterior pole in the left eye (Figure 1E). While early phase fluorescein angiography in the left eye showed small hyperfluorescent retinal spots (Figure 1F), the right eye appeared normal on funduscopy or fluorescein angiography. SD-OCT in the left eye revealed a disrupted IS/OS line in the foveal region (Figure 2B). There was no evidence of systemic inflammation and no therapy was administered.

Subjective visual improvement was reported within several days from the onset of the symptom. VA recovered to 1.2 six days after the initial visit, and after one month the foveal granularity and yellow-white spots had disappeared entirely (Figure 1G) and the IS/OS line was restored. At the final visit (133 days after the initial visit), VA was 1.5 and the IS/OS line in the left eye was found to be preserved (Figure 2D). The simvastatin treatment has been continued during the follow-up period.

Assessment of subfoveal choroidal and central retinal thickness

In Patient 1, while the subfoveal choroidal thickness at the initial visit (acute phase) was 337 µm in the affected right eye (Figures 2A and 3A), this thickness markedly decreased to 249 µm at 133 days after the initial visit (convalescent phase) and measured 243 µm on the final visit (345 days after the initial visit) (Figure 3A). The subfoveal choroidal thickness in the opposite left eye also decreased over the course of follow up, from 277 µm to 241 µm (Figure 3A).

Similarly, in Patient 2, the subfoveal choroidal thickness at the initial visit (acute phase) was 440 µm in the affected left eye (Figures 2B and 3B) but markedly

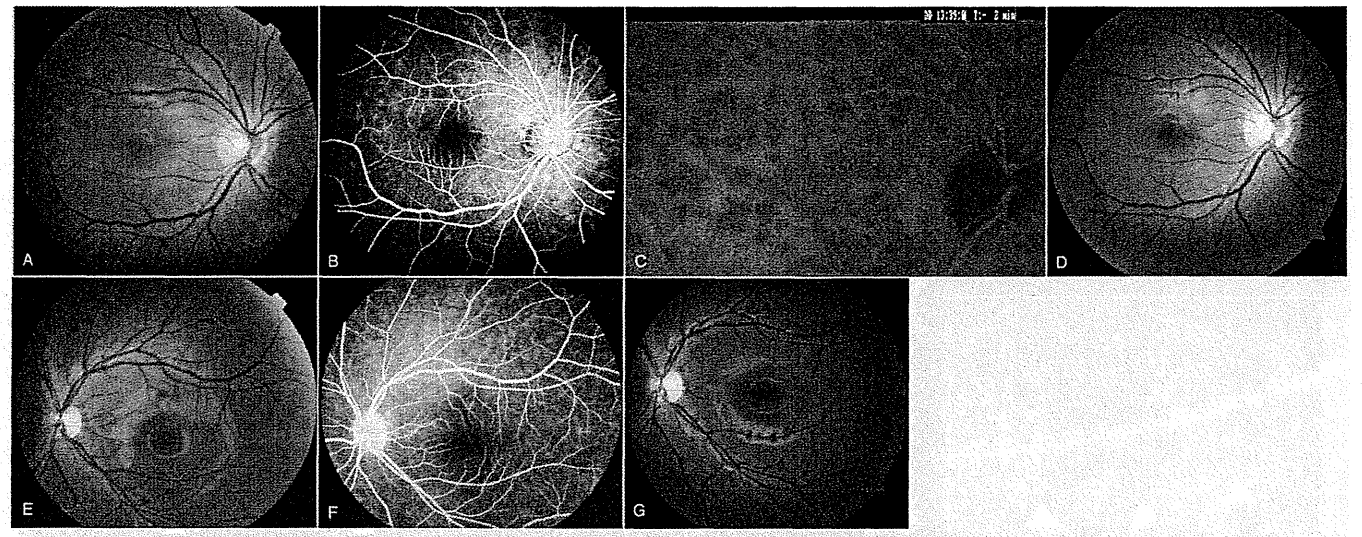

Figure 1. Fundus images of the right eye of Patient 1 (A–D) and the left eye of Patient 2 (E–G).
Fundus photograph showing foveal granularity and scattered yellow-white spots in the posterior pole (A). Early phase fluorescein angiographic image showing small hyperfluorescent retinal spots (B). Late-phase indocyanine green angiographic image showing numerous hypofluorescent spots throughout the posterior pole (C). Fundus photograph showing that the foveal granularity and yellow-white spots had disappeared at five weeks after the initial visit (D). Fundus photograph showing foveal granularity and faint, scattered, yellow-white spots in the posterior pole (E). Early phase fluorescein angiographic image showing small hyperfluorescent retinal spots (F). Fundus photograph showing that the foveal granularity and yellow-white spots had disappeared one month after the initial visit (G).

decreased to 358 µm at the final visit (133 days after the initial visit, convalescent phase) (Figures 2D and 3B). The subfoveal choroidal thickness in the opposite eye (RE) also decreased, from 382 µm to 331 µm (Figure 3B).

In both patients, the choroidal stromal vessels in the acute phase (Figures 2A and 2B) were more dilated than in the convalescent phase (Figures 2C and 2D); however, no change was noted in the central retinal thickness of either eye of either patient (Figures 3C and 3D for Patients 1 and 2, respectively) during the follow-up periods.

DISCUSSION

Here, we report new SD-OCT findings in two patients with MEWDS. The subfoveal choroidal thickness in patients during the acute phase was considerably thicker than in the convalescent phase, not only in the affected eye but also in the asymptomatic opposite eye. In addition, thickness during the acute phase was thicker in the affected eye than in the opposite eye in both patients.

Although the aetiology of MEWDS is not well understood, fluorescein angiographic and electrophysiological studies have suggested that this inflammatory disease affects the retinal pigment epithelium and outer retina. Subsequently, several reports have suggested that the numerous hypofluorescent spots noted on ICGA are likely to be due to hypoperfusion of the choriocapillaris, making the disease primary inflammation of the choriocapillaris.[11,12] Schaal and colleagues[13] reported a single case of simultaneous appearance of MEWDS and multifocal choroiditis, suggesting a possible common causal entity.

In contrast to indocyanine green angiographic findings, recent SD-OCT studies have noted no abnormalities in the retinal pigment epithelial layer or choroid in MEWDS patients,[8,9] although choroidal thickness has not been compared between the acute and convalescent phases. SD-OCT findings for affected eyes in the present study revealed a marked decrease in subfoveal choroidal thickness from the acute phase without therapy in both patients after four or more months (Figures 2 and 3). A recent study described electroretinographic and SD-OCT findings in seven patients with MEWDS,[7] noting that the choroidal thickness and the choroidal stromal vessels in the convalescent phase (four months after the initial visit) appeared to be reduced over values in the acute phase in at least one (Patient 1 in Figure 2[7]) of the seven patients, although the authors did not explicitly mention choroidal thickness.[7] The SD-OCT findings in our two patients showed greater dilation in the choroidal stromal vessels during the acute phase (Figures 2A and 2B) compared with the convalescent phase (Figures 2C and 2D),

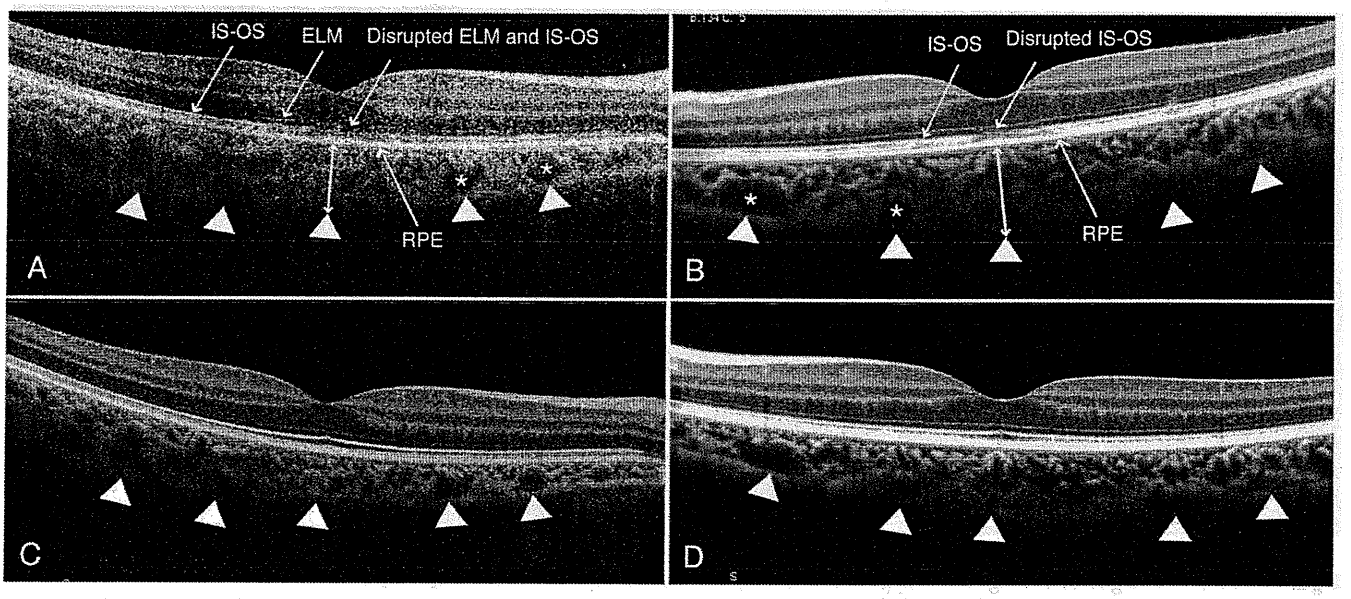

Figure 2. Horizontal scan images (6.0 mm) of spectral-domain optical coherence tomography (SD-OCT) of the right eye of Patient 1 (A and C) and the left eye of Patient 2 (B and D).
The SD-OCT images reveal a disrupted external limiting membrane (ELM) and photoreceptor inner segment/outer segment junction (IS/OS) lines in the foveal region (A) and a disrupted IS/OS line in the foveal region (B) in the acute phase. The asterisks indicate dilated choroidal stromal vessels (A and B). The SD-OCT images show restoration of the ELM line and IS/OS lines at the final visit (345 days after the initial visit) (C) and restoration of the IS/OS line at the final visit (133 days after the initial visit) (D) in the convalescent phase. The arrowheads indicate the choroid/sclera junction (A–D). The double-headed arrows indicate subfoveal choroidal thickness (A and B). The subfoveal choroidal thickness markedly decreased from 337 μm (A) to 249 μm (C) in Patient 1 and from 440 μm (B) to 358 μm (D) in Patient 2.

suggesting that choroidal thickening might be due to dilation of the choroidal stromal vessels. These present and previous findings suggest that in addition to a disrupted IS/OS line, choroidal thickening might be a feature of the acute phase of MEWDS (Figures 2A and 2B).[7–9]

Marked increases in choroidal thickness can be observed in patients with Vogt–Koyanagi–Harada (VKH) disease[14] or central serous chorioretinopathy (CSC).[15,16] VKH disease is a bilateral granulomatous uveitis, in which the target of the inflammatory reaction is located within the choroidal stroma, making the disease primary stromal choroiditis.[17] While the increased choroidal thickness in VKH disease might be related to inflammatory infiltration or increased exudation,[14] the thickening in central serous chorioretinopathy, which is characterised by an idiopathic and mostly unilateral serous retinal detachment in the posterior pole,[18] has been confirmed to be due to choroidal vascular hyperpermeability.[15,16] While typically seen in patients with VKH or CSC, no leakage or hyperpermeability of choroidal stromal vessels is noted with indocyanine green angiography in the acute phase of MEWDS;[12,19] however, several studies[4,20] of MEWDS patients have reported focal segmental staining of choroidal vessels and discrete nodular hyperfluorescent areas in the inner choroid with ICGA. Taken together, these findings suggest that an inflammatory reaction might also occur at the level of the choroidal stroma in addition to the choriocapillaris.

In most patients with MEWDS, recovery of visual function occurs within several weeks.[19] Interestingly, Patient 2, who had simvastatin treatment, reported a more rapid improvement in both symptoms and visual acuity. Simvastatin belongs to the class of cholesterol-lowering statins. It has been proposed that statins have anti-inflammatory effects that are not directly related to their cholesterol-lowering activity.[21,22] Although anti-inflammatory effects of statins have not been demonstrated in inflammatory choroidal disease, the rapid visual improvement in Patient 2 might be associated with simvastatin treatment.

Explaining why choroidal thickening was observed even in the asymptomatic opposite eyes in the present study is difficult (Figures 3A and 3B). A recent study[7] observed that five of seven patients with unilateral MEWDS manifested visual field abnormalities in both eyes, not just the affected eyes, during the acute phase, suggesting that visual dysfunction is bilateral

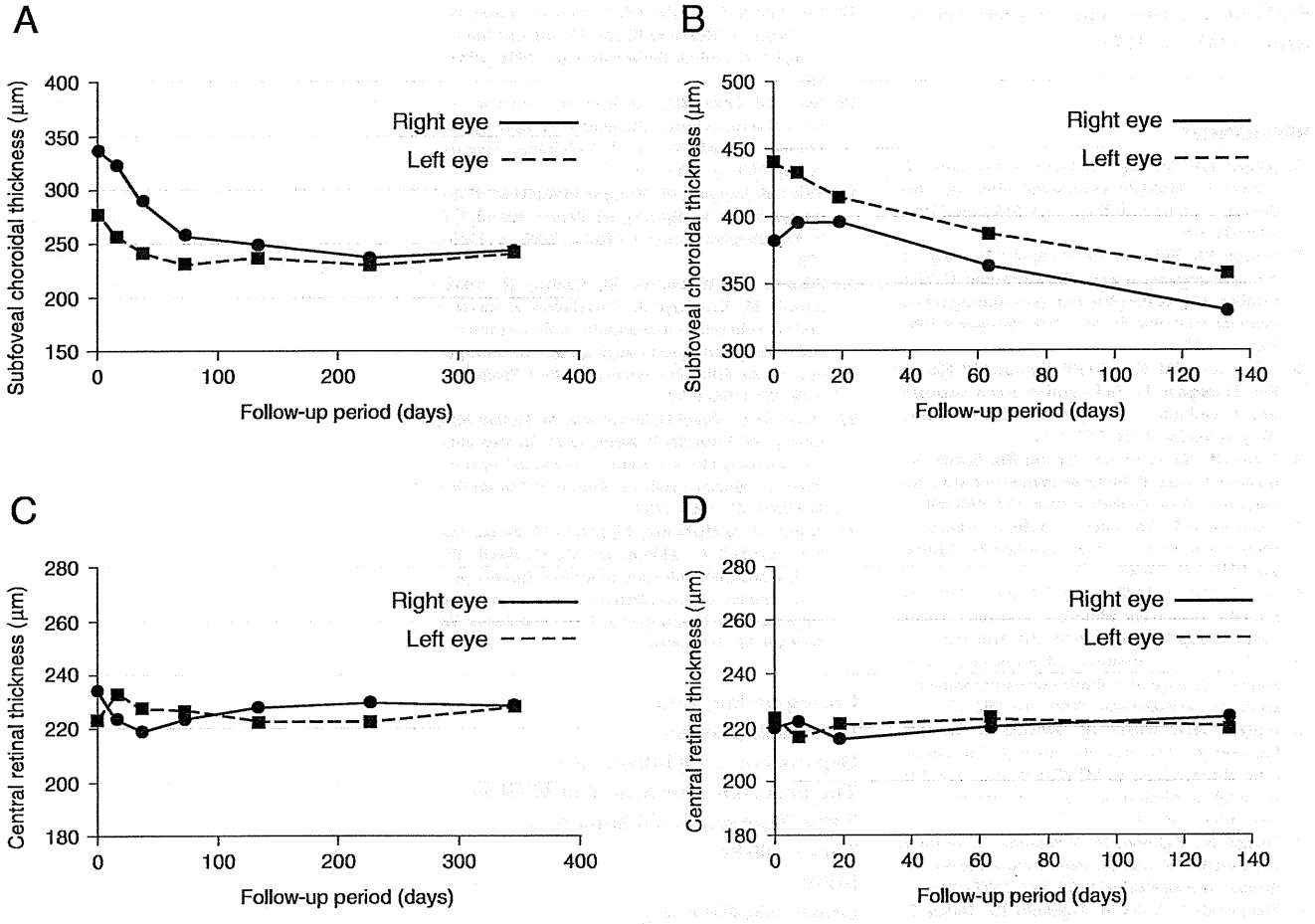

Figure 3. Changes in subfoveal choroidal thickness (A and B) and central retinal thickness (C and D) during the follow-up period for Patients 1 (A and C) and 2 (B and D).

In Patient 1, the subfoveal choroidal thickness at the initial visit (day zero, acute phase) in the right eye was 337 μm (A), markedly decreased to 249 μm (day 133, convalescent phase) and was 243 μm at the final visit (Day 345) (A). The thickness in the left eye (asymptomatic opposite eye) also decreased from 277 μm (day zero) to 241 μm (day 345) (A). Similarly, in Patient 2, the subfoveal choroidal thickness at the initial visit (day zero, acute phase) in the left eye was 440 μm (B) and markedly decreased to 358 μm at the final visit (day 133, convalescent phase) (B). The thickness in the right eye (asymptomatic opposite eye) also decreased from 382 μm (day zero) to 331 μm (day 133) (B). No changes were noted in central retinal thickness for either eye of Patients 1 (C) or 2 (D) during the follow-up period.

in most patients. Given these present and previous findings, the inflammatory reaction in MEWDS might occur bilaterally more often than unilaterally, even though the condition is believed to be unilateral in most patients.

In conclusion, this is the first report to describe the relationship between subfoveal choroidal thickness and MEWDS. We noted the previously unreported finding that choroid thickness was greater in the acute phase than in the convalescent phase in both eyes, not just the affected eyes, suggesting that an inflammatory reaction might occur in the choroidal stroma in addition to the choriocapillaris. Because our findings were derived from only two patients, further study is needed to determine the presence of choroidal thickening in other patients with MEWDS.

GRANTS AND FINANCIAL SUPPORT

This study was supported by grants from the Ministry of Education, Culture, Sports, Science and Technology of Japan (Grant-in-Aid for Scientific Research) (TH), The Jikei University Research Fund (TH) and

the Vehicle Racing Commemorative Foundation (TH and HT).

REFERENCES

1. Jampol LM, Sieving PA, Pugh D, Fishman GA, Gilbert H. Multiple evanescent white dot syndrome. I. Clinical findings. *Arch Ophthalmol* 1984; 102: 671–674.
2. Sieving PA, Fishman GA, Jampol LM, Pugh D. Multiple evanescent white dot syndrome. II. Electrophysiology of the photoreceptors during retinal pigment epithelial disease. *Arch Ophthalmol* 1984; 102: 675–679.
3. Ie D, Glaser BM, Murphy RP, Gordon LW, Sjaarda RN, Thompson JT. Indocyanine green angiography in multiple evanescent white-dot syndrome. *Am J Ophthalmol* 1994; 117: 7–12.
4. Gross NE, Yannuzzi LA, Freund KB, Spaide RF, Amato GP, Sigal R. Multiple evanescent white dot syndrome. *Arch Ophthalmol* 2006; 124: 493–500.
5. Laatikainen L, Immonen I. Multiple evanescent white dot syndrome. *Graefes Arch Clin Exp Ophthalmol* 1988; 226: 37–40.
6. Feigl B, Haas A, El-Shabrawi Y. Multifocal ERG in multiple evanescent white dot syndrome. *Graefes Arch Clin Exp Ophthalmol* 2002; 240: 615–621.
7. Li D, Kishi S. Restored photoreceptor outer segment damage in multiple evanescent white dot syndrome. *Ophthalmology* 2009; 116: 762–770.
8. Nguyen MH, Witkin AJ, Reichel E, Ko TH, Fujimoto JG, Schuman JS, Duker JS. Microstructural abnormalities in MEWDS demonstrated by ultrahigh resolution optical coherence tomography. *Retina* 2007; 27: 414–418.
9. Hangai M, Fujimoto M, Yoshimura N. Features and function of multiple evanescent white dot syndrome. *Arch Ophthalmol* 2009; 127: 1307–1313.
10. Manjunath V, Taha M, Fujimoto JG, Duker JS. Choroidal thickness in normal eyes measured using Cirrus HD optical coherence tomography. *Am J Ophthalmol* 2010; 150: 325–329.
11. Herbort CP. Inflammatory choriocapillaropathies: general concepts. In: Gupta A, Gupta G, Herbort CP, Khairallah M, eds. Uveitis Text and Imaging. New Delhi: Jaypee Brothers Medical Publishers, 2009. p 430–441.
12. Herbort CP. Multiple evanescent white dot syndrome (MEWDS) and acute idiopathic blind spot enlargement (AIBSE). In: Gupta A, Gupta G, Herbort CP, Khairallah M, eds. Uveitis Text and Imaging. New Delhi: Jaypee Brothers Medical Publishers, 2009. p 441–447.
13. Schaal S, Schiff WM, Kaplan HJ, Tezel TH. Simultaneous appearance of multiple evanescent white dot syndrome and multifocal choroiditis indicate a common causal relationship. *Ocul Immunol Inflamm* 2009; 17: 325–327.
14. Maruko I, Iida T, Sugano Y, Oyamada H, Sekiryu T, Fujiwara T, Spaide RF. Subfoveal choroidal thickness after treatment of Vogt–Koyanagi–Harada disease. *Retina* 2011; 31: 510–517.
15. Imamura Y, Fujiwara T, Margolis R, Spaide RF. Enhanced depth imaging optical coherence tomography of the choroid in central serous chorioretinopathy. *Retina* 2009; 29: 1469–1473.
16. Maruko I, Iida T, Sugano Y, Ojima A, Ogasawara M, Spaide RF. Subfoveal choroidal thickness after treatment of central serous chorioretinopathy. *Ophthalmology* 2010; 117: 1792–1799.
17. Bouchenaki N, Herbort CP. Stromal choroiditis. In: Pleyer U, Mondino B, eds. Uveitis and Immunological Disorders. Berlin. Springer, 2004. p 233–253.
18. Klais CM, Ober MD, Ciardella AP, Yannuzzi LA. Central serous chorioretinopathy. In: Ryan SJ, ed. Retina. 4th ed. Vol 2. Philadelphia: Elsevier Mosby, 2006. p 1135–1161.
19. Tsai LM, Jampol LM. Multiple evanescent white-dot syndrome. In: Ryan SJ, ed. Retina. 4th ed. Vol 2. Philadelphia: Elsevier Mosby, 2006. p 1785–1791.
20. Sikorski BL, Wojtkowski M, Kaluzny JJ, Szkulmowski M, Kowalczyk A. Correlation of spectral optical coherence tomography with fluorescein and indocyanine green angiography in multiple evanescent white dot syndrome. *Br J Ophthalmol* 2008; 92: 1552–1557.
21. Diomede L, Albani D, Sottocorno M, Donati MB, Bianchi M, Fruscella P, Salmona M. In vivo anti-inflammatory effect of statins is mediated by non-sterol mevalonate products. *Arterioscler Thromb Vasc Biol* 2001; 21: 1327–1332.
22. Bartoli M, Al-Shabrawey M, Labazi M, Behzadian MA, Istanboli M, El-Remessy AB, Cardwell AW et al HMG-CoA reductase inhibitors (statin) prevents retinal neovascularization in a model of oxygen-induced retinopathy. *Invest Ophthalmol Vis Sci* 2009, 50: 4934–4940.

Corresponding author:
Dr Takaaki Hayashi
Department of Ophthalmology
The Jikei University School of Medicine
3-25-8 Nishi-shimbashi Minato-ku
Tokyo, 105-8461
JAPAN
E-mail: taka@jikei.ac.jp

Int Ophthalmol (2011) 31:471–475
DOI 10.1007/s10792-011-9479-z

CASE REPORT

Color vision in an elderly patient with protanopic genotype and successfully treated unilateral age-related macular degeneration

Takaaki Kitakawa · Takaaki Hayashi · Satoshi Tsuzuranuki · Akiko Kubo · Hiroshi Tsuneoka

Received: 13 October 2010 / Accepted: 8 March 2011 / Published online: 11 November 2011

Abstract We investigated differences in color discrimination between the fellow eye and the affected eye successfully treated for unilateral age-related macular degeneration (AMD) in a 69-year-old male patient with protanopia. His best-corrected visual acuity (BCVA) was 1.2 in the right eye (RE) and 0.2 in the left eye (LE). Fundus and angiographic findings showed classic choroidal neovascularization (CNV) secondary to AMD in the LE. BCVA of the LE improved to 0.4, and CNV resolved by 15 months after initiating combined anti-vascular endothelial growth factor and photodynamic therapies. After CNV closure, the Farnsworth dichotomous was performed, showing confusion patterns of the protan axis in either eye. The Farnsworth-Munsell 100-hue test showed a total error score of 520 in the LE, much higher than the score of 348 in the RE. Complete genotypes of the long-wavelength-sensitive (L−) cone and middle-wavelength-sensitive (M−) cone opsin genes were determined by polymerase chain reaction, revealing that the patient had a single 5′ L–M 3′ hybrid gene (encoding an M-cone opsin), with this genotype responsible for protanopia (the L-cone opsin gene was non-functional), instead of the L-cone and M-cone opsin gene arrays. Poorer color vision discrimination in the LE than the RE remained present despite closure of CNV. The presence and type of congenital color vision defect can be confirmed using molecular genetic testing even if complications of acquired retinal diseases such as AMD are identified.

Keywords Age-related macular degeneration · Choroidal neovascularization · Color vision defects · Molecular genetics · Genetic analysis

T. Kitakawa · T. Hayashi (✉) · S. Tsuzuranuki · H. Tsuneoka
Department of Ophthalmology, The Jikei University School of Medicine, 3-25-8, Nishi-shimbashi, Minato-ku, Tokyo 105-8461, Japan
e-mail: taka@jikei.ac.jp

A. Kubo
Department of Ophthalmology, Kinan Hospital, Mie, Japan

Introduction

Age-related macular degeneration (AMD) is the leading cause of severe vision loss in older adults in developed countries. Recent studies have shown that the combination of anti-vascular endothelial growth factor (VEGF) therapy and photodynamic therapy (PDT) is effective against choroidal neovascularization (CNV) due to AMD [1]. Distance visual acuity assessment is the most commonly used method to evaluate visual function in AMD patients, and few reports have assessed color vision after treatment for AMD. This is due to the difficulty in adequately evaluating color discrimination in AMD patients

≥65 years of age, particularly as such patients often have diabetes in addition to senile cataracts.

Congenital color vision defects such as X-linked recessively inherited and non-progressive disorders are common [2], with an incidence of approximately 8% in Caucasian men and 5% in Japanese men. The presence of congenital color vision defects cannot therefore be ignored for assessing color vision in AMD patients.

This report investigated differences in color discrimination between the fellow eye and the affected eye successfully treated for AMD in a male patient with protanopia (one type of dichromacy in congenital color vision defects) diagnosed by molecular genetic analysis.

Case report

This study was approved by the institutional review board of The Jikei University School of Medicine. The protocol adhered to the tenets of the Declaration of Helsinki, and informed consent was obtained from the patient.

A 69-year-old man became aware of distorted vision and loss of visual acuity in May 2007, and presented to our department on August 16, 2007. The patient had long history of smoking and a medical history of diabetes mellitus, hypertension, hyperlipidemia, arrhythmia and congenital color blindness. On initial evaluation, decimal best-corrected visual acuity (BCVA) was 1.2 in the right eye (RE) and 0.2 in the left eye (LE). No abnormalities were found except mild cataracts in the anterior segments and media of both eyes. Intraocular pressure was 13 mmHg bilaterally. Fundoscopy showed no notable abnormalities in the RE (Fig. 1a), but a subfoveal grayish-yellow lesion with subretinal hemorrhage in the LE (Fig. 1b). Fluorescein angiography of the LE showed hyperfluorescence in the foveal area due to leakage from predominantly classic CNV secondary to AMD (Fig. 1c). Indocyanine green angiography showed focal hyperfluorescence in the area corresponding to the CNV (Fig. 1d). Optical coherence tomography (OCT) (OCT3 Stratus; Carl Zeiss Meditec AG, Dublin, CA, USA) showed the appearance of the normal foveal depression in the RE (Fig. 1e), and confirmed the presence of subfoveal CNV in the LE (Fig. 1f). The patient underwent verteporfin (Visudyne®; Novartis AG, Bülach, Switzerland) PDT 2 weeks after the first visit. Three months later, combined therapy comprising verteporfin PDT and intravitreal injection of bevacizumab (Avastin®, 1.25 mg/0.05 ml; Genentech, South San Francisco, CA, USA), a non-selective VEGF inhibitor, was initiated to treat persistent CNV. At the 3-month follow-up, no persistent or recurrent CNV was identified on angiography or OCT. BCVA of the LE improved to 0.4 and CNV resolved (Fig. 1g) by 15 months after starting combined therapy. At this time, color vision was assessed monocularly using the Farnsworth Dichotomous Test (panel D-15) and the Farnsworth-Munsell 100-hue (F-M 100-hue) test. The result for panel D-15 showed confusion patterns of the protan axis in both LE (Fig. 2a) and RE (Fig. 2b). The F-M 100-hue test revealed a total error score (TES) of 520 in the LE (Fig. 2c), much higher than the score of 348 in the RE (Fig. 2d). Regarding orientation axes, the RE indicated a significant red–green axis, whereas the LE indicated both red–green and blue–yellow axes.

For molecular genetic analysis, genomic DNA was isolated from whole blood. Genotype of the long-wavelength-sensitive (L) cone and middle-wavelength-sensitive (M) cone opsin genes was completely determined by polymerase chain reaction and sequencing as previously reported [2–4]. In normal male trichromats, L- and M-opsin genes are arranged in a head-to-tandem array (Fig. 3) on the X chromosome, whereas this patient showed a single 5′ L–M 3′ hybrid gene (encoding an M opsin) (Fig. 3) with the genotype responsible for protanopia [2]. The L-opsin gene was thus non-functioning in this patient.

Discussion

Determining which type of congenital color vision defects is present in elderly patients is difficult using standard color vision tests alone, as aging, cataracts and age-related maculopathy all affect color discrimination. In fact, our patient had senile cataracts, diabetes and unilateral AMD in addition to congenital color vision defects.

Previous studies have shown that TES for the F-M 100 hue test is significantly higher in elderly subjects than in younger subjects [5, 6]. Diabetic patients with minimal or even no diabetic retinopathy also show significantly higher mean TES for the F-M 100 hue

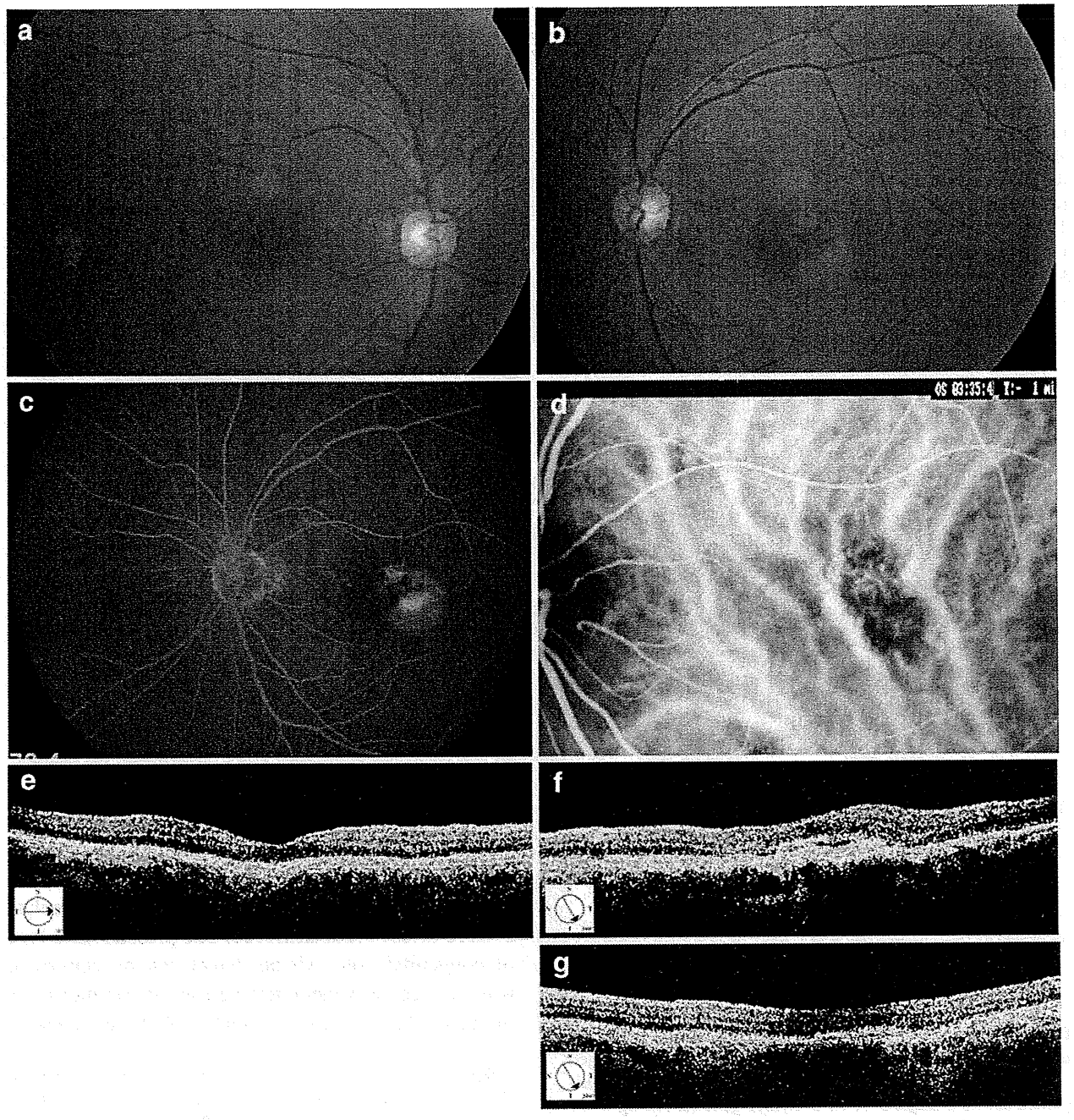

Fig. 1 Images from fundoscopy (**a**, **b**), mid-phase fluorescein angiography (FA) (**c**), mid-phase indocyanine green angiography (ICGA) (**d**) and optical coherence tomography (OCT) (**e**, **f**, **g**) in the patient. Fundoscopy shows no notable abnormalities in the right eye (**a**), but a subfoveal grayish-yellow lesion with subretinal hemorrhage in the left eye (**b**). FA of the left eye shows hyperfluorescence in the foveal area due to leakage from predominantly classic choroidal neovascularization (CNV) (**c**). ICGA of the left eye shows focal hyperfluorescence in the area corresponding to the CNV (**d**). OCT shows the appearance of the normal foveal depression in the right eye (**e**), subfoveal CNV in the left eye (**f**), and the resolved CNV (**g**) in the left eye at 15 months after starting combined therapy

test than age-matched normal controls [7, 8]. Those studies have identified increased lens density, aging and diabetes as factors affecting color discrimination.

We have already identified genotype–phenotype correlations in male subjects with congenital color vision defects [2, 9]. In the present patient, the type of

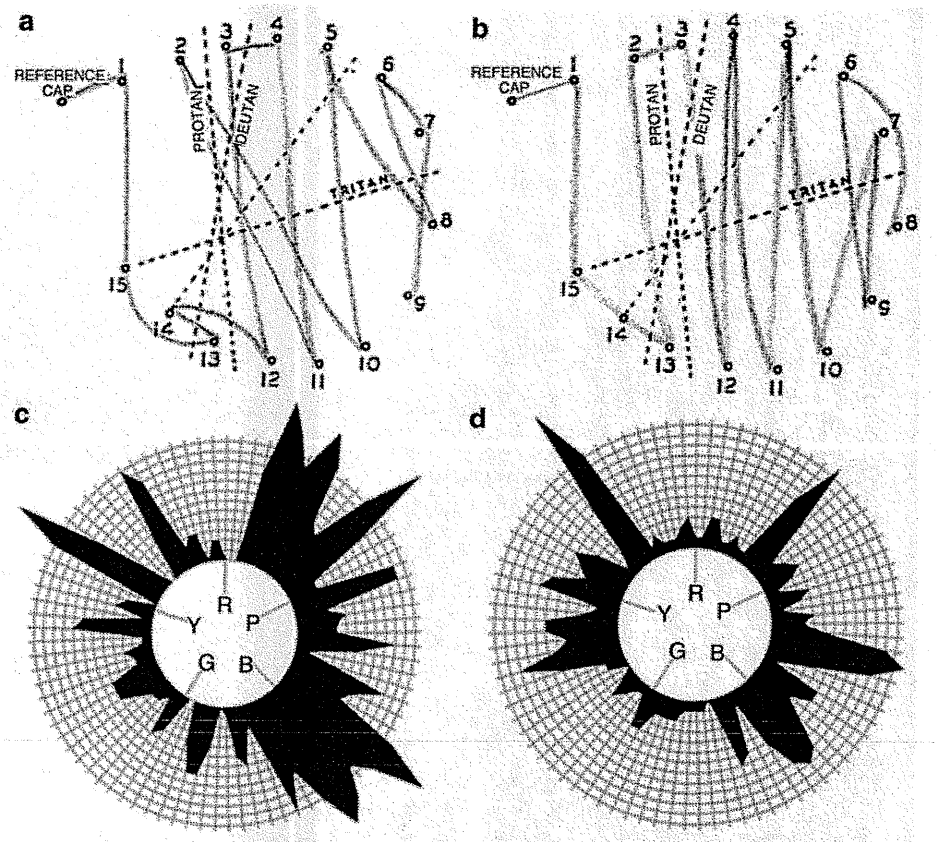

Fig. 2 Results of the Farnsworth Dichotomous Test (Panel D-15) test (**a**, **b**), the Farnsworth-Munsell 100-hue (F-M 100-hue) test (**c**, **d**). Panel D-15 results show confusion patterns of the protan axis in the left (**a**) and right eyes (**b**). F-M 100-hue results show total error scores of 520 in the left eye (**c**) and 348 in the right eye (**d**)

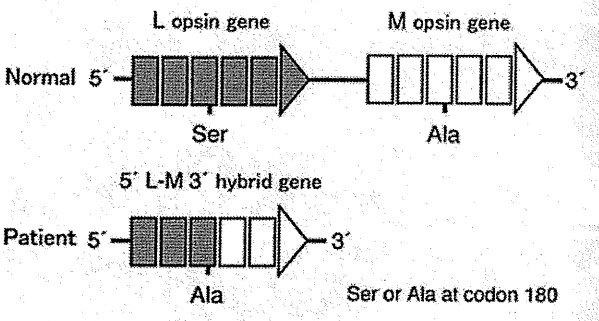

Fig. 3 Genotype of the L- and M-opsin gene array. In normal male trichromats (Normal), L- and M-opsin genes are arranged in a head-to-tandem array on the X chromosome, whereas this patient shows a single 5′ L–M 3′ hybrid gene (encoding an M opsin), with this genotype being responsible for protanopia

congenital color vision defects was diagnosed as protanopia by molecular genetic analysis (Fig. 3). When color discrimination was compared between the fellow eye and the affected eye, conditions (age, senile cataracts, diabetes and protanopia) were equivalent between eyes. Results of the F-M 100-hue test revealed poorer color discrimination in the LE (Fig. 2c) than in the RE (Fig. 2d). Differences in color discrimination between the eyes were attributed to the resolved unilateral CNV confirmed by angiography and OCT. Poorer color discrimination in the LE than in the RE is thus likely to be due to loss of function of all three cone classes in the fovea.

In conclusion, poorer color discrimination in the LE than in the RE was due to AMD, for which complete closure of CNV was achieved. The presence and type of congenital color vision defect can be confirmed using molecular genetic testing even if complications of acquired retinal diseases such as AMD are present.

Acknowledgments This work was supported by grants from The Jikei University Research Fund (T.H.) and the Vehicle Racing Commemorative Foundation (T.H. and H.T.).

References

1. Dhalla MS, Shah GK, Blinder KJ, Ryan EH Jr, Mittra RA, Tewari A (2006) Combined photodynamic therapy with verteporfin and intravitreal bevacizumab for choroidal neovascularization in age-related macular degeneration. Retina 26:988–993. doi:10.1097/01.iae.0000247164.70376.91
2. Deeb SS, Hayashi T, Winderickx J, Yamaguchi T (2000) Molecular analysis of human red/green visual pigment gene

locus: relationship to color vision. Methods Enzymol 316:651–670
3. Young TL, Deeb SS, Ronan SM et al (2004) X-linked high myopia associated with cone dysfunction. Arch Ophthalmol 122:897–908. doi:10.1001/archopht.122.6.897
4. Hayashi T, Kubo A, Takeuchi T, Gekka T, Goto-Omoto S, Kitahara K (2006) Novel form of a single X-linked visual pigment gene in a unique dichromatic color-vision defect. Vis Neurosci 23:411–417. doi:10.1017/S0952523806233029
5. Verriest G, Van Laethem J, Uvijls A (1982) A new assessment of the normal ranges of the Farnsworth-Munsell 100-hue test scores. Am J Ophthalmol 93:635–642
6. Beirne RO, McIlreavy L, Zlatkova MB (2008) The effect of age-related lens yellowing on Farnsworth-Munsell 100 hue error score. Ophthalmic Physiol Opt 28:448–456. doi:10.1111/j.1475-1313.2008.00593.x
7. Roy MS, Gunkel RD, Podgor MJ (1986) Color vision defects in early diabetic retinopathy. Arch Ophthalmol 104:225–228
8. Hardy KJ, Lipton J, Scase MO, Foster DH, Scarpello JH (1992) Detection of colour vision abnormalities in uncomplicated type 1 diabetic patients with angiographically normal retinas. Br J Ophthalmol 76:461–464
9. Jagla WM, Jagle H, Hayashi T, Sharpe LT, Deeb SS (2002) The molecular basis of dichromatic color vision in males with multiple red and green visual pigment genes. Hum Mol Genet 11:23–32

Graefes Arch Clin Exp Ophthalmol (2011) 249:201–208
DOI 10.1007/s00417-010-1482-y

RETINAL DISORDERS

A novel mutation (Cys83Tyr) in the second zinc finger of *NR2E3* in enhanced S-cone syndrome

Amândio Rocha-Sousa · Takaaki Hayashi · Nuno Lourenço Gomes · Susana Penas · Elisete Brandão · Paulo Rocha · Mitsuyoshi Urashima · Hisashi Yamada · Hiroshi Tsuneoka · Fernando Falcão-Reis

Received: 30 October 2009 / Revised: 25 July 2010 / Accepted: 26 July 2010 / Published online: 20 August 2010

Abstract
Background Enhanced S-cone syndrome (ESCS) is an autosomal recessive retinal disorder characterized by an increased number of S-cones over L/M cones and rods. Mutations in the *NR2E3* gene, encoding a photoreceptor-specific nuclear receptor, are identified in patients with ESCS. The purpose of this study is to report the ophthalmic features of a 25-year-old Portuguese male with a typical ESCS phenotype and a novel homozygous *NR2E3* mutation.
Methods The patient underwent a detailed ophthalmic examination including fundus photography, fluorescein angiography (FAF), fundus autofluorescence imaging (FAI), and spectral domain optical coherence tomography (SD-OCT). Full-field electroretinography (ERG), S-cone ERG, and multifocal ERG were performed. Mutation screening of the *NR2E3* gene was performed with polymerase chain reaction amplification and direct sequencing.
Results The patient had poor visual acuity but good color vision. Funduscopy showed degenerative changes from the vascular arcades to the midperipheral retina. The SD-OCT revealed macular schisis and cystoid changes that had no fluorescein leakage. The posterior pole showed diffusely increased autofluorescence compared with eccentric areas in both eyes. International-standard full-field ERG showed the typical pathognomonic changes associated with ESCS and the short-wavelength flash ERG was simplified, delayed, and similar to the standard photopic flash ERG. Multifocal ERG showed widespread delay and reduction. Genetic analysis revealed a novel homozygous mutation (p.C83Y), which resides in the second zinc finger of the DNA-binding domain.
Conclusions This homozygous mutation is likely to affect binding to target DNA sites, resulting in a non-functional behavior of NR2E3 protein. It is associated

Presented at the EVER 2006 Meeting, Vilamoura, Portugal

A. Rocha-Sousa (✉) · N. L. Gomes · S. Penas · E. Brandão · P. Rocha · F. Falcão-Reis
Department of Ophthalmology, Hospital de São João, Porto, Portugal
e-mail: arsousa@med.up.pt

N. L. Gomes
e-mail: nunolgomes@gmail.com

S. Penas
e-mail: spenas75@yahoo.com

E. Brandão
e-mail: elisetebrandao@netcabo.pt

P. Rocha
e-mail: prochax@gmail.com

F. Falcão-Reis
e-mail: falcaor@med.up.pt

A. Rocha-Sousa
Physiology Department, Faculty of Medicine, University of Porto, Porto, Portugal

T. Hayashi · H. Tsuneoka
Department of Ophthalmology, The Jikei University School of Medicine, Tokyo, Japan

T. Hayashi
e-mail: takaaki@amy.hi-ho.ne.jp

M. Urashima
Division of Molecular Epidemiology, The Jikei University School of Medicine, Tokyo, Japan
e-mail: urashima@jikei.ac.jp

H. Yamada
Department of Molecular Genetics, Institute of DNA Medicine, The Jikei University School of Medicine, Tokyo, Japan
e-mail: hyamad@jikei.ac.jp

with a typical form of ESCS with a nondetectable rod response and reduced/delayed mfERG responses at all eccentricities.

Keywords Enhanced S-cone syndrome, NR2E3 · S-cone · Retina · ERG

Introduction

Most retinal dystrophies are the result of either a generalized rod dysfunction, a generalized cone dysfunction (involving all three cone subtypes), or a generalized dysfunction of both rods and cones either simultaneously or successively. In 1990, Marmor [1] described a series of eight patients with night blindness, cystoid maculopathy, degenerative changes in the region of the vascular arcades, and loss of visual field. These patients showed S-cone hypersensitivity in electrophysiological testing; this condition was designated enhanced S-cone syndrome (ESCS). The ESCS has an autosomal recessive inheritance pattern and is characterized by hypersensitivity to short wavelength flashes with a concomitant decreased rod and L and M cone response [1–3].

Over ten mutations of the *NR2E3* gene have been identified in European patients with ESCS [4]. This gene encodes a photoreceptor-specific nuclear receptor. It consists of eight exons mapped on chromosome 15q24 [5]. Functionally, *NR2E3* protein regulates the proper differentiation and maturation of rod and cone photoreceptors [6–10]. To date, more than 30 mutations in the *NR2E3* gene have been described not only in ESCS [4, 11–15] but also in Goldmann–Favre syndrome (GFS) [11, 16], autosomal recessive retinitis pigmentosa [17, 18], autosomal dominant retinitis pigmentosa [17, 19], and clumped pigmentary retinal degeneration [11]. Because appropriate ERG analyses demonstrated a relatively enhanced S-cone function and the presence of *NR2E3* mutations in GFS, it was concluded that the two diseases are likely to be one clinical entity, being the GFS the severe phenotype [11, 16, 20].

Although characteristic electroretinographic responses are usually essential for diagnosis, there is a variable spectrum of disease severity in patients with ESCS. We describe the clinical findings of a Portuguese patient with ESCS with a novel homozygous mutation in the *NR2E3* gene and exhibited a typical phenotype.

Materials and methods

Clinical studies

Ophthalmic examination included best-corrected visual acuity (BCVA), slit-lamp and dilated fundus observation, Goldmann kinetic perimetry, chromatic vision testing, fluorescein angiogram (FAF), fundus autofluorescence imaging (FAI), spectral domain optical coherence tomography (SD-OCT), contrast sensitivity, dark adaptometry, and electrophysiological testing. Color vision testing included color contrast sensitivity threshold and the Farnsworth 100-hue test. The color contrast sensitivity thresholds were measured as proposed by Arden et al. (1988). In brief, the system uses a calibrated 21-inch color monitor to present random letters as targets to be identified. The letters are of equal luminance to the background, and can only be recognized because their hue differs from the background. All stimuli are equiluminant with the background. This is ensured by a preliminary adjustment (in every patient) of the relative luminance of the red and green and green and blue phosphors. Then a modified binary search is carried out to determine the threshold color contrast along the protan, deuteran, and tritan color confusion lines [21]. All these color vision tests were performed monocularly. Cross-sectional retinal images were evaluated using SD-OCT (SPECTRALIS Spectral-domain OCT, Heidelberg Engineering, Heidelberg, Germany). The SD-OCT was taken horizontally through the fovea (transverse width of 20°). Dark adaptometry was performed based on the Goldman-Weeker adaptometer. Briefly, the patient was pre-adapted under photopic conditions (30 cd/m^2) for 5 min. The dark adaptation characteristic was then assessed by measuring detection thresholds under scotopic conditions over a 30-min period.

Electrophysiological evaluation included full-field electroretinograms (ERG) using a Ganzfeld dome, long duration ON-OFF ERG, S-cone ERG, Electro-oculogram (EOG), and multifocal ERG (mf ERG). The ERG testing was performed according to the protocol of the International Society for Clinical Electrophysiology of Vision [22]. Briefly, under dilation and after dark adaptation (30 min), a dim white flash of 0.01-0.05 cd·s/m^2 was used for the scotopic (rod) response and a single white bright-flash (3 cd·s/m^2) for the combined response. After light adaptation (10 min; 25 cd/m^2), a brief white flash (3 cd·s/m^2) was superimposed for the photopic response. The 30-Hz ERG was obtained in the same conditions using a 30-Hz flickering stimulation. The S-cone ERG was performed, under photopic conditions, using a blue stimulus (440 nm; 10 ms; 65 cd/m^2) on an orange (660 nm; 350 cd/m^2) background [23, 24]. For the L/M cones ON-OFF ERG, the 200-ms orange (660 nm; 350 cd/m^2) stimulus was used on a green (530 nm; 130 cd/m^2) background [25]. The EOG was obtained after a room light pre-adaptation period of 10 min [26]. Acquisitions were made after 15 min of dark adaptation and repeated after 15 min of light adaptation. The mfERG was acquired using an array of 61 stimulus (200 cd/m^2) according to the recommendations of ISCEV [27]. All the electrophysiological exams were performed using the Metrovision

vision monitor (Pérenchies, France). For the ON-OFF ERG and the S-cone ERG, an additional external led stimulator was used (CH electronics).

Molecular genetic studies

The protocol adhered to the Declaration of Helsinki, and informed consent was obtained from the participant. Genetic analysis was performed at the Department of Ophthalmology at The Jikei University as previously described [12, 15]. Briefly, genomic DNA was extracted from venous blood samples using a Puregene Blood DNA Isolation kit (Gentra Systems, Minneapolis, MN). For mutation screening, all exons (exon 1 to exon 8) and the promoter region of the *NR2E3* gene were amplified by polymerase chain reaction (PCR) using previously reported primers [12, 15]. The PCR products were purified with a QIAquick PCR Purification kit (Qiagen, Tokyo, Japan) and used as the template for sequencing. Both strands were sequenced on an automated sequencer (3730*xl* DNA Analyzer, Applied Biosystems, Foster City, CA) using a BigDye Terminator kit V3.1 (Applied Biosystems). A nucleotide variation in exon 3 was analyzed in 100 normal controls without any retinal diseases.

Results

Clinical findings

A 25-year-old male patient was referred to our hospital with suspected X-linked juvenile retinoschisis. The patient was one of the three children from a consanguineous couple (second-degree cousins) and was the only family member with visual symptoms. His chief complaint was of decreased vision but, even after inquiry, he denied nyctalopia. His BCVA was 0.5 in

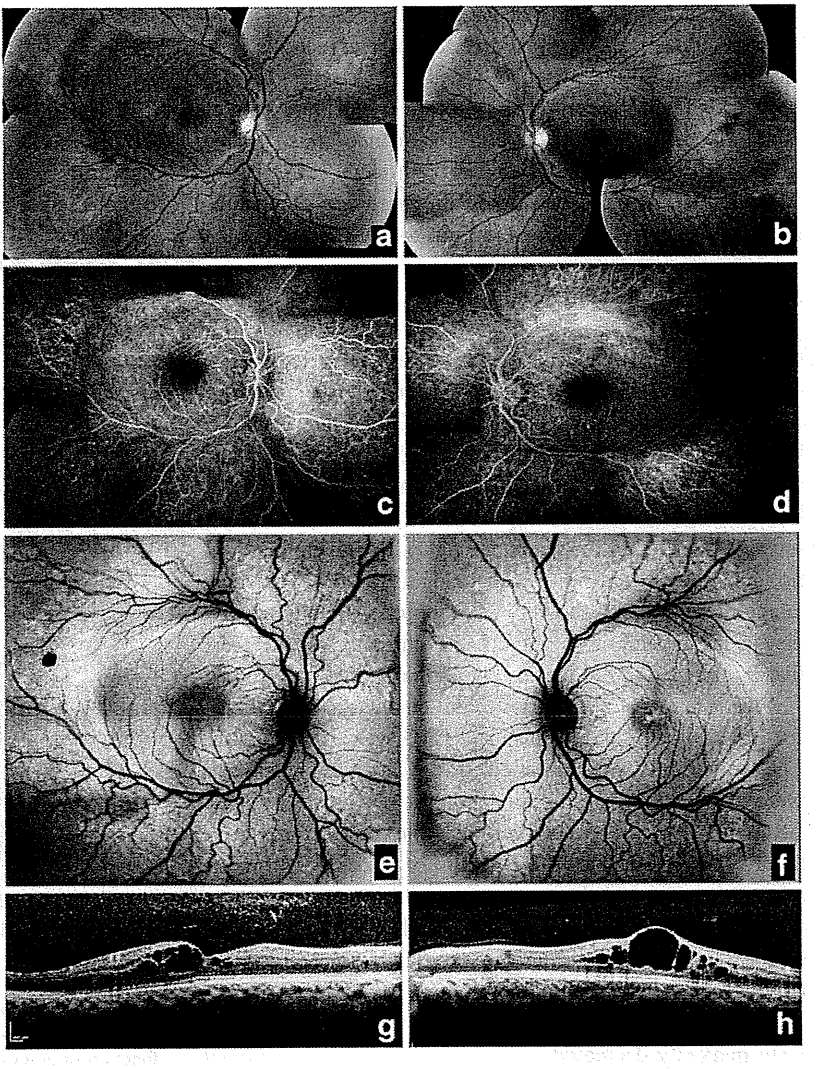

Fig. 1 Fundus photographs and fluorescein angiograms (FAF) images. Color fundus montages of the right eye (**a**) and left eye (**b**) show degenerative lesions in the midzonal retinal areas, near the arcades with nummular pigmentary changes at the RPE level. Absence of foveal reflex and the presence of schisis-like changes in both maculae are also observed. Midphase fluorescein angiograms of the right eye (**c**) and left eye (**d**) show no leakage in the maculas. The fundus autofluorescence images (**e** and **f**) show a diffusely increased auto fluorescence (AF) associated with the arcades with some sparing of central and inferior macular area. The SD-OCT images show the presence of macular schisis with cystoid changes in the right (**g**) and left maculas (**g**) in the inner and outer nuclear layers

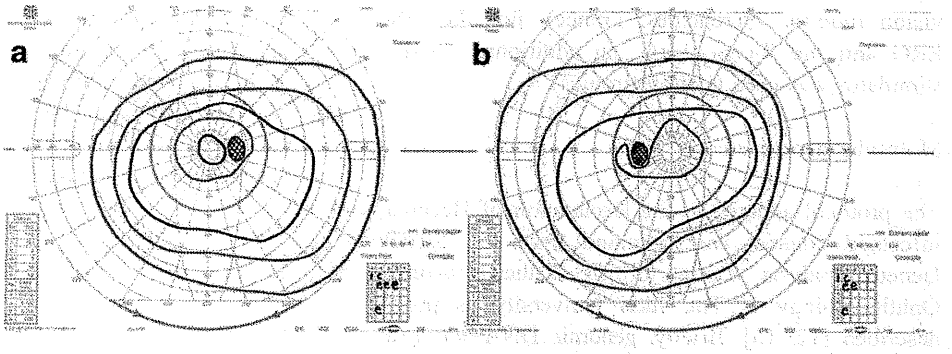

Fig. 2 Goldmann perimetry shows decreased central sensitivity with constriction of the I/2e and/or I/3e isopters (**a** 1/2e: 10° of fixation in the right and **b** I/3e: 20° of fixation in the left), but normal peripheral visual fields

the right eye and 0.25 in the left eye. The anterior segment examination was unremarkable. Intraocular pressure was within the normal range. Fundoscopy showed bilateral foveal schisis-like changes (Fig. 1a, b). In addition, nummular pigmentary deposits were observed at the RPE level in the mid-periphery and along the vascular arcades, without vascular attenuation. FAF did not reveal any hyperfluorescence or leakage at the macular lesions (Fig. 1c, d). FAI showed diffusely increased AF over broad, crescent-like areas associated with the vascular arcades and optic disc in both eyes. More eccentric areas were hypofluorescent in comparison. Parafoveal hyperfluorescence was greater in the left eye compared to the right eye (Fig. 1e, f). The SD-OCT images confirmed the presence of macular schisis with cystoid changes in both maculae (Fig. 1g, h).

Functional evaluation

Color vision testing did not demonstrate a preferred axis of chromatic confusion, with 100 and 186 error scores in the right and left eye respectively on the Farnsworth 100-hue. The CCS thresholds were within normal limits. Goldmann perimetry revealed bilaterally decreased central sensitivity with constriction of the I/2e and/or I/3e isopters (I/3e: 20° of fixation in the left and 1/2e: 10° of fixation in the right). However, there was no constriction of the visual fields (Fig. 2). The dark adaptometry curve showed a monophasic pattern with elevated cone threshold without the characteristic decrease that is attributed to rod function in normal individuals (Fig. 3).

Electrodiagnostic tests revealed characteristic patterns for ESCS. Scotopic dim flash rod ERG were undetectable. The waveforms of combined (rod-plus-cone) responses were similar to those of the photopic responses. Flicker ERGs of 30-Hz were smaller than the single flash cone a-waves (Fig. 4). The ERG results of specific chromatic stimulation showed that most of the ERG responses were arising from S-cone systems. S-cone ERG were delayed, simplified, and resemble the single flash cone ERG (Fig. 5). The ON-OFF responses with 200-ms orange stimulation, which are originated from the L/M cones [23], were markedly decreased in the patient, indicating minimal responses to L/M cone stimulation (Fig. 5). The OFF L/M cones response was absent.

The EOG light rise was detected, with a reduction on the Arden index (1.56 and 1.65, for a normal value of 1.85).

Comparing the mf ERG to the mf ERG of normal subjects, reduced amplitudes and delayed implicit times, of both N1 and P1 components, were observed at all eccentricities and at all retinal locations (Fig. 6).

Molecular genetic findings

The genetic analysis identified a novel homozygous mutation in exon 3. This mutation leads to the substitution of an adenine for a guanine base (c.248G>A). At the proteic level, this causes the substitution of a tyrosine for a cysteine at position 83 on the highly conserved DNA-binding

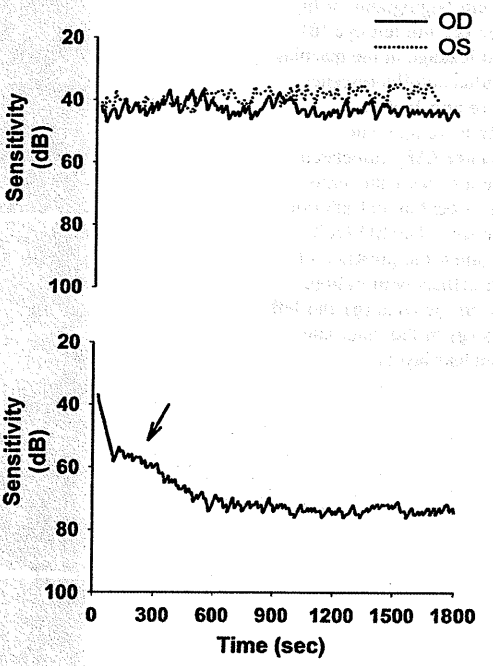

Fig. 3 Dark adaptometry curve of the patient (*upper panel*) shows a monophasic pattern without the characteristic decline attributed to rod function (*arrow*) that is seen in normal individuals (*lower panel*)

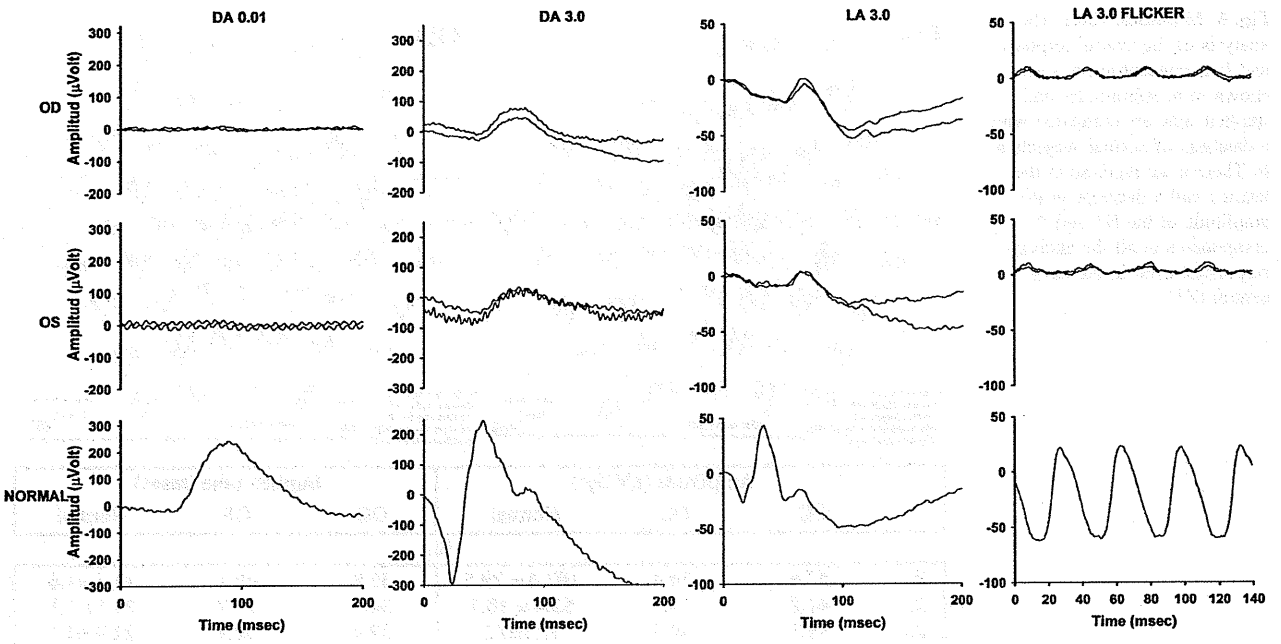

Fig. 4 Full-field electroretinograms (ERGs) of the patient and a normal subject. In the patient, there is no scotopic response (DA 0.01); the waveforms of the combined (DA 3.0) and photopic (LA 3.0) ERGs are very similar. The photopic ERG a-and b-waves are delayed almost 20 ms when compared to the normal subject. Delayed 30-Hz flicker ERG (LA 3.0 flicker), with lower amplitude than the single-flash photopic a-wave are also detected

domain (DBD), which consists of 84 amino acids (cysteine 47 to valine 130) (Fig. 7). No other nucleotide substitution was detected in the patient. The cysteine residue at position 83 (Cys83) within the second zinc finger motif of the DBD (arrow) is conserved among orthologs of other vertebrate species (Fig. 7), predicting a functionally important amino acid residue.

The patient's parents were heterozygotes for the mutation (p.C83Y). This mutation was not found in the 100 normal controls or in database searches of PubMed, The Human Gene Mutation Database (URL: http://www.hgmd.cf.ac.uk/), and of the Leiden Open Variation Database (http://www.lovd.nl/) [20].

Discussion

In this study, we describe the clinical, electrophysiological, and psychophysical findings of a 25-year-old male patient who was diagnosed with ESCS. Genetic analysis revealed a novel homozygous *NR2E3* mutation (p.C83Y). This is the first report of an ESCS patient with any *NR2E3* mutation in the Portuguese population.

The DBD of NR2E3 is composed of highly conserved two zinc finger motifs that facilitate binding to target DNA sites [19]. Four cysteine residues are coordinated with one zinc atom in each zinc finger. Cys83 is the first cysteine residue of the second zinc finger (Cys83 to Cys103) [19].

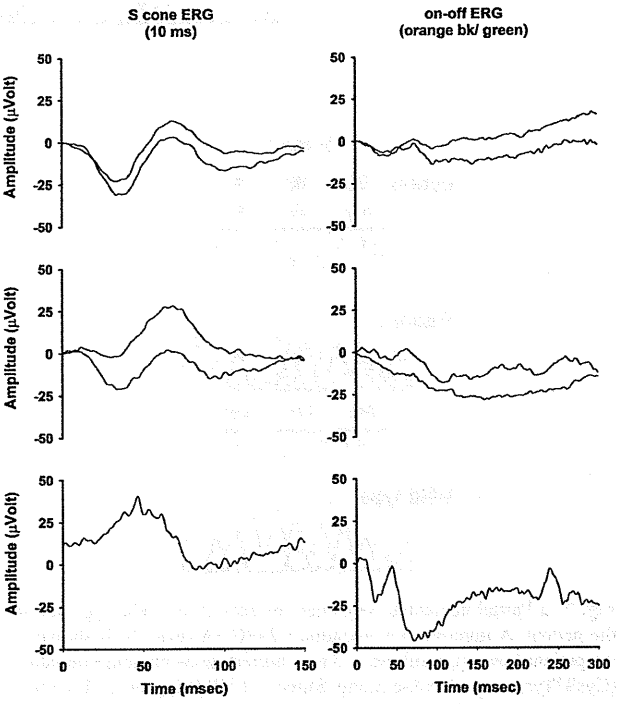

Fig. 5 Electroretinograms of specific chromatic stimulation. S-cone ERGs were delayed, simplified, and resemble the single flash cone ERGs. The ON-OFF responses with 200-ms orange stimulation are markedly decreased. The S-cone ERGs waveforms were not superimposable due to limited patient compliance

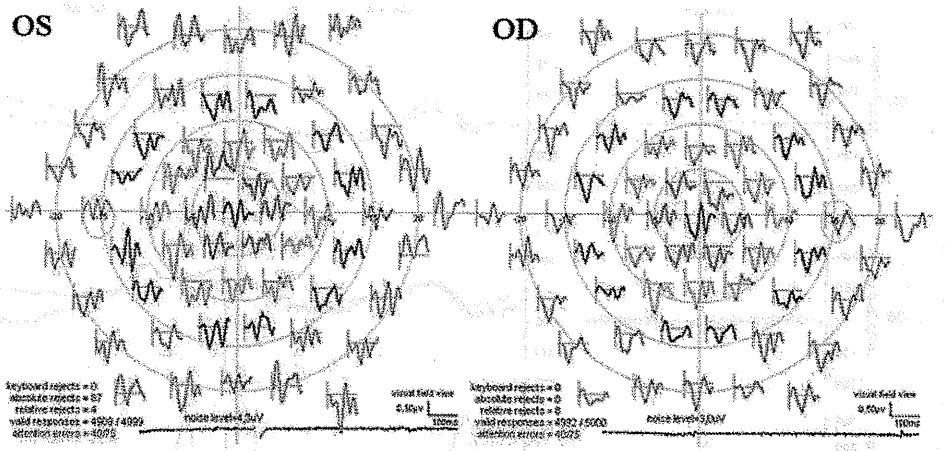

Fig. 6 Multifocal ERG. The analysis of the central response and four concentric rings are shown in **a**. Amplitudes and implicit time are compared with a database of normal subjects in **b**. There is an increase in the latency and a decrease in the amplitude of the N1 and P1 components in all the analyzed responses, even in the most central (Z1)

	Amplitude (nV/dg^2)			Implicit time (msec)		
	OD	OS	Normal	OD	OS	Normal
			N_1			
Z_1	57.6	34.4	102.4 ± 29.5	35.8	40.1	23.7 ±1.6
Z_2	41.8	15.7	53.4 ± 10.7	34.1	37.7	23.5 ±1.1
Z_3	31.5	30.9	37.7±7.2	37.4	36.4	22.9 ±1.1
Z_4	18.5	18.9	28.3 ± 5.5	40.1	38.0	22.8 ±1.2
Z_5	15.9	11.7	22 ± 4.4	41.0	39.0	23.1 ±1.2
			P_1			
Z_1	79.6	56.1	165.0 ± 40.0	54.6	56.9	46.4 ± 2.4
Z_2	40.9	32.2	100.1 ± 18.6	54.9	57.2	42.5 ±1.3
Z_3	34.1	29.7	69.3 ± 13.0	58.2	57.7	41.1 ± 1.4
Z_4	20.7	20.4	52.4 ± 10.6	62.9	58.3	40.4 ±1.4
Z_5	15.9	14.2	41.3 ± 9.0	63.6	64.1	40.6± 1.5

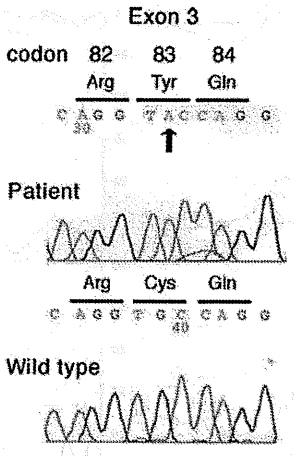

Fig. 7 **a** Partial nucleotide sequences of exon 3 in a wild-type and in the patient. A homozygous variation c.248G>A (exon 3) is shown in the patient (*arrow*), resulting in a new homozygous missense mutation (Cys83Tyr) in the DNA-binding domain of NR2E3 protein. **b** Amino acid alignment of the DNA binding domain of the human NR2E3 protein. The cysteine residue at position 83 within the second zinc finger motif (*arrow*) is highly conserved among orthologs of human NR2E3. hs: *Homo sapiens* (human); mm: *Mus musculus* (mouse); gg: *Gallus gallus* (chicken); xt: *Xenopus tropicalis* (xenopus); dr: *Danio rerio* (zebrafish)

The D-box, a short loop with six amino acid residues between the first cysteine (Cys83) and second cysteine (Cys90) of the second zinc finger [5], is important for homodimerization of NR2E3 to be functionally active, suggesting that Cys83 is an important amino acid. In vitro experiments using electrophoretic mobility shift assay showed that varied NR2E3 proteins with mutations in the zinc finger motifs exhibited reduced binding to the target DNA sites [28, 29]. Those NR2E3 mutant proteins, which were localized at least partially in cell nuclei, exhibited reduced transcriptional activity of the target gene [28, 29] and impaired dimerization [29] using cultured cells. The p. C83Y mutated NR2E3 protein is not able to dimerize to become active. This results in disruption of the target DNA binding sites leading to a null function of the DBD. It is expected that the homozygous p.C83Y mutation causes severe non-functional behavior of NR2E3 protein.

ESCS shares several clinical features with GFS that is characterized by night blindness, pigmentary degeneration, macular and peripheral retinoschisis, posterior subcapsular cataract, markedly abnormal ERG and degenerative vitreous changes [30, 31]. Jacobson et al. demonstrated enhanced S-cone responses in patients with GFS [3], while *NR2E3* mutations have been also found in GFS patients. Based on these findings, it was concluded that these two diseases are

likely to be one clinical entity [11], with two identifiable phenotypes in a wide-range spectrum of clinical expression of the same retinal degeneration [16, 20]. However, the absence of peripheral retinoschisis, posterior subcapsular cataract, and degenerative vitreous changes differentiates ESCS patients from patients with GFS phenotype. Our patient did not exhibit peripheral retinoschisis, cataract, or degenerative vitreous changes. The SD-OCT images revealed macular schisis with cystoid changes (Fig. 1), which are frequently seen in both ESCS and GFS [11, 16, 24] but are different from cystoid macular edema secondary to other conditions such as diabetic retinopathy and retinal vein occlusion that are characterized by the presence of leakage on fluorescein angiography.

The main ERG characteristics in our patient included the pathognomonic changes previously described in [24]. This included an absent rod ERG consistent with absence of rods. There was a simplified and delayed waveform to a standard flash under photopic and scotopic conditions, presumably both dominated by short-wavelength sensitive cones. The 30-Hz flicker ERG was severely abnormal and delayed and was smaller than the single flash cone ERG a-wave; these distinctive findings may be explained by considering the low temporal resolution of the S-cone system.

These results are in accordance with the histopathological studies that have demonstrated the absence of rods and the predominance of S-cone opsin over L/M cones in postmortem retinas of ESCS patients [32, 33]. Mild phenotypes of ESCS associated with compound heterozygous mutations have been found to have a residual rod response or a morphologically normal waveform of the combined ERG, either alone or together [15, 34]. Regarding the mfERG findings, Marmor et al. [35] previously described a normal waveform in the most central ring and a marked deterioration in the two paracentral rings in a patient with ESCS. Subsequently, similar mfERG findings have been described in five patients with ESCS, at least two of which had macular cysts [24]. Thus most of the patients had nearly normal central response [24, 35], suggesting preserved function of the most central macula retina in ESCS. However, our patient showed reduced amplitudes with delayed implicit times in both N1 and P1 components even in the most central ring (Z1) of both eyes (Fig. 6). The disorganization of laminar structure, namely macular schisis with cystoid changes (Fig. 1) can explain the reduced amplitudes of all the ring of the mfERG (Fig. 6). The condition of our patient with the homozygous p.C83Y mutation, causing expression of the putative non-functional NR2E3 protein, may be associated with a severer phenotype of ESCS that has reduced central mfERG responses compared with that of ESCS with preserved central responses.

In summary, we reported the first Portuguese ESCS patient with a novel homozygous mutation (p.C83Y) in the *NR2E3* gene. The mutation, which resides within the second zinc finger of the DBD, may cause a typical form of ESCS with nondetectable rod responses and reduced mfERG amplitudes in all eccentricities.

Acknowledgments This work was supported by grants from the Sociedade Portuguesa de Oftalmologia, from the Ministry of Education, Culture, Sports, Science and Technology of Japan [Grant-in-Aid for Scientific Research (C) #19592042] (TH) and the Vehicle Racing Commemorative Foundation (TH and HT).

References

1. Marmor MF, Jacobson SG, Foerster MH, Kellner U, Weleber RG (1990) Diagnostic clinical findings of a new syndrome with night blindness, maculopathy, and enhanced S-cone sensitivity. Am J Ophthalmol 110:124–134
2. Jacobson SG, Marmor MF, Kemp CM, Knighton RW (1990) SWS (blue) cone hypersensitivity in a newly identified retinal degeneration. Invest Ophthalmol Vis Sci 31:827–838
3. Jacobson SG, Roman AJ, Roman MI, Gass JD, Parker JA (1991) Relatively enhanced S-cone function in the Goldmann–Favre syndrome. Am J Ophthalmol 111:446–453
4. Haider NB, Jacobson SG, Cideciyan AV, Swiderski R, Streb LM, Searby C, Beck G, Hockey R, Hanna DB, Gorman S, Duhl D, Carmi R, Bennett J, Weleber RG, Fishman GA, Wright AF, Stone EM, Sheffield VC (2000) Mutation of a nuclear receptor gene, NR2E3, causes enhanced S-cone syndrome, a disorder of retinal cell fate. Nat Genet 24:127–131
5. Kobayashi M, Takezawa S, Hara K, Yu RT, Umesono Y, Agata K, Taniwaki M, Yasuda K, Umesono K (1999) Identification of a photoreceptor cell-specific nuclear receptor. Proc Natl Acad Sci USA 96:4814–4819
6. Haider NB, Naggert JK, Nishina PM (2001) Excess cone cell proliferation due to lack of a functional NR2E3 causes retinal dysplasia and degeneration in rd7/rd7 mice. Hum Mol Genet 10:1619–1626
7. Cheng H, Khanna H, Oh EC, Hicks D, Mitton KP, Swaroop A (2004) Photoreceptor-specific nuclear receptor NR2E3 functions as a transcriptional activator in rod photoreceptors. Hum Mol Genet 13:1563–1575. doi:10.1093/hmg/ddh173
8. Peng GH, Ahmad O, Ahmad F, Liu J, Chen S (2005) The photoreceptor-specific nuclear receptor Nr2e3 interacts with Crx and exerts opposing effects on the transcription of rod versus cone genes. Hum Mol Genet 14:747–764
9. Cheng H, Aleman TS, Cideciyan AV, Khanna R, Jacobson SG, Swaroop A (2006) In vivo function of the orphan nuclear receptor NR2E3 in establishing photoreceptor identity during mammalian retinal development. Hum Mol Genet 15:2588–2602. doi:10.1093/hmg/ddl185
10. Haider NB, Demarco P, Nystuen AM, Huang X, Smith RS, McCall MA, Naggert JK, Nishina PM (2006) The transcription factor Nr2e3 functions in retinal progenitors to suppress cone cell generation. Vis Neurosci 23:917–929
11. Sharon D, Sandberg MA, Caruso RC, Berson EL, Dryja TP (2003) Shared mutations in NR2E3 in enhanced S-cone syndrome, Goldmann–Favre syndrome, and many cases of clumped pigmentary retinal degeneration. Arch Ophthalmol 121:1316–1323
12. Nakamura Y, Hayashi T, Kozaki K, Kubo A, Omoto S, Watanabe A, Toda K, Takeuchi T, Gekka T, Kitahara K (2004) Enhanced S-cone syndrome in a Japanese family with a nonsense NR2E3 mutation (Q350X). Acta Ophthalmol Scand 82:616–622
13. Nakamura M, Hotta Y, Piao CH, Kondo M, Terasaki H, Miyake Y (2002) Enhanced S-cone syndrome with subfoveal neovascularization. Am J Ophthalmol 133:575–577

14. Wright AF, Reddick AC, Schwartz SB, Ferguson JS, Aleman TS, Kellner U, Jurklies B, Schuster A, Zrenner E, Wissinger B, Lennon A, Shu X, Cideciyan AV, Stone EM, Jacobson SG, Swaroop A (2004) Mutation analysis of NR2E3 and NRL genes in enhanced S-cone syndrome. Hum Mutat 24:439
15. Hayashi T, Gekka T, Goto-Omoto S, Takeuchi T, Kubo A, Kitahara K (2005) Novel NR2E3 mutations (R104Q, R334G) associated with a mild form of enhanced S-cone syndrome demonstrate compound heterozygosity. Ophthalmology 112:2115
16. Pachydaki SI, Klaver CC, Barbazetto IA, Roy MS, Gouras P, Allikmets R, Yannuzzi LA (2009) Phenotypic features of patients with NR2E3 mutations. Arch Ophthalmol 127:71–75. doi:10.1001/archophthalmol.2008.534
17. Escher P, Gouras P, Roduit R, Tiab L, Bolay S, Delarive T, Chen S, Tsai CC, Hayashi M, Zernant J, Merriam JE, Mermod N, Allikmets R, Munier FL, Schorderet DF (2009) Mutations in NR2E3 can cause dominant or recessive retinal degenerations in the same family. Hum Mutat 30:342–351. doi:10.1002/humu.20858
18. Gerber S, Rozet JM, Takezawa SI, dos Santos LC, Lopes L, Gribouval O, Penet C, Perrault I, Ducroq D, Souied E, Jeanpierre M, Romana S, Frezal J, Ferraz F, Yu-Umesono R, Munnich A, Kaplan J (2000) The photoreceptor cell-specific nuclear receptor gene (PNR) accounts for retinitis pigmentosa in the Crypto-Jews from Portugal (Marranos), survivors from the Spanish Inquisition. Hum Genet 107:276–284
19. Coppieters F, Leroy BP, Beysen D, Hellemans J, De Bosscher K, Haegeman G, Robberecht K, Wuyts W, Coucke PJ, De Baere E (2007) Recurrent mutation in the first zinc finger of the orphan nuclear receptor NR2E3 causes autosomal dominant retinitis pigmentosa. Am J Hum Genet 81:147–157. doi:10.1086/518426
20. Schorderet DF, Escher P (2009) NR2E3 mutations in enhanced S-cone sensitivity syndrome (ESCS), Goldmann–Favre syndrome (GFS), clumped pigmentary retinal degeneration (CPRD), and retinitis pigmentosa (RP). Hum Mutat 30:1475–1485. doi:10.1002/humu.21096
21. Arden G, Gunduz K, Perry S (1988) Color vision testing with a computer graphics system: preliminary results. Doc Ophthalmol 69:167–174
22. Marmor MF, Fulton AB, Holder GE, Miyake Y, Brigell M, Bach M (2009) ISCEV Standard for full-field clinical electroretinography (2008 update). Doc Ophthalmol 118:69–77. doi:10.1007/s10633-008-9155-4
23. Arden G, Wolf J, Berninger T, Hogg CR, Tzekov R, Holder GE (1999) S-cone ERGs elicited by a simple technique in normals and in tritanopes. Vision Res 39:641–650
24. Audo I, Michaelides M, Robson AG, Hawlina M, Vaclavik V, Sandbach JM, Neveu MM, Hogg CR, Hunt DM, Moore AT, Bird AC, Webster AR, Holder GE (2008) Phenotypic variation in enhanced S-cone syndrome. Invest Ophthalmol Vis Sci 49:2082–2093. doi:10.1167/iovs.05-1629
25. Khan NW, Jamison JA, Kemp JA, Sieving PA (2001) Analysis of photoreceptor function and inner retinal activity in juvenile X-linked retinoschisis. Vision Res 41:3931–3942
26. Brown M, Marmor M, Vaegan ZE, Brigell M, Bach M (2006) ISCEV Standard for Clinical Electro-oculography (EOG) 2006. Doc Ophthalmol 113:205–212. doi:10.1007/s10633-006-9030-0
27. Hood DC, Bach M, Brigell M, Keating D, Kondo M, Lyons JS, Palmowski-Wolfe AM (2008) ISCEV guidelines for clinical multifocal electroretinography (2007 edition). Doc Ophthalmol 116:1–11. doi:10.1007/s10633-007-9089-2
28. Kanda A, Swaroop A (2009) A comprehensive analysis of sequence variants and putative disease-causing mutations in photoreceptor-specific nuclear receptor NR2E3. Mol Vis 15:2174–2184
29. Roduit R, Escher P, Schorderet DF (2009) Mutations in the DNA-binding domain of NR2E3 affect in vivo dimerization and interaction with CRX. PLoS One 4:e7379. doi:10.1371/journal.pone.0007379
30. Peyman GA, Fishman GA, Sanders DR, Vlchek J (1977) Histopathology of Goldmann–Favre syndrome obtained by full-thickness eye-wall biopsy. Ann Ophthalmol 9:479–484
31. Nasr YG, Cherfan GM, Michels RG, Wilkinson CP (1990) Goldmann–Favre maculopathy. Retina 10:178–180
32. Ben-Arie-Weintrob Y, Berson EL, Dryja TP (2005) Histopathologic-genotypic correlations in retinitis pigmentosa and allied diseases. Ophthalmic Genet 26:91–100
33. Milam AH, Rose L, Cideciyan AV, Barakat MR, Tang WX, Gupta N, Aleman TS, Wright AF, Stone EM, Sheffield VC, Jacobson SG (2002) The nuclear receptor NR2E3 plays a role in human retinal photoreceptor differentiation and degeneration. Proc Natl Acad Sci USA 99:473–478
34. Lam BL, Goldberg JL, Hartley KL, Stone EM, Liu M (2007) Atypical mild enhanced S-cone syndrome with novel compound heterozygosity of the NR2E3 gene. Am J Ophthalmol 144:157–159. doi:10.1016/j.ajo.2007.03.012
35. Marmor MF, Tan F, Sutter EE, Bearse MA Jr (1999) Topography of cone electrophysiology in the enhanced S-cone syndrome. Invest Ophthalmol Vis Sci 40:1866–1873